Pursuit - The Journal of Undergraduate Research at The University of Tennessee

Volume 11 | Issue 1 Article 2

July 2022

Synthesis and Consolidation of the Aluminosilicate Mineral Anorthite

Lauren E. Eccles
University of Tennessee, Knoxville, leccles@vols.utk.edu

1. Introduction

Synthetic silicate minerals can be processed from sustainable raw materials to achieve properties, structures, high purity, and homogeneity not found in their natural counterparts. Synthetic minerals can be advantageous compared to natural minerals for at least two important reasons: (1) synthetic mineral crystal structure and composition can be carefully controlled; and (2) microstructure and morphology can be controlled via processing conditions. Thus, synthetic minerals are used in a variety of technological applications. For instance, synthetic cationic clay minerals have numerous biomedical applications, including pharmaceuticals, cosmetics, regenerative medicine [1] and drug delivery [2]. Synthetic clay (e.g., LAPONITE®, a synthetic smectite clay [1]) and synthetic zeolites [3] are also being used to adsorb and separate pollutants from liquids, such as heavy metals from wastewater. Synthetic minerals with exotic structures also find application in catalytic reaction applications. For instance, self-assembled, nano-scale, artificial allophane spherules (allophane is an aluminosilicate similar to kaolinite) are used as a platform for constructing integrated nano-catalysts [4].

In the study presented here, the interest is in fabricating a synthetic feldspar. Feldspars are common constituents in granite, while granitic mineral assemblages are some of the most important components in concrete. The goal is to fabricate a feldspar, selected as a *model* mineral constituent of concrete, with controlled composition and microstructure in accordance with the long-range goal to investigate the radiation damage properties of this model mineral phase, particularly in how radiation damage relates to assessing the durability of the concrete used in the biological shield walls within nuclear reactor pressure vessels.

Feldspar mineral phases have been successfully synthesized in several studies published in the literature. For instance, in 1950, Goldsmith [5] reported substituting gallium and germanium for

aluminum and silicon, respectively, in synthetic feldspars. This work was key to characterizing cationic arrangements in feldspars using X-ray diffraction (XRD). Without the heavy atom substitution of Ga and Ge for Al and Si, XRD is incapable of distinguishing the lattice site occupancies of Al and Si in the feldspar crystal structure. Flehmig [6] in 1977 successfully synthesized potassium feldspars, as well as albites and plagioclases, at very low temperatures using aqueous solution hydroxide gel synthesis procedures. Additionally, in 2007 Pöter et al. [7], produced a novel synthetic feldspar known as buddingtonite, $NH_4[AlSi_3O_8]$. This phase is crystallographically similar to potassium feldspar, except that all of the K^+ cations in potassium feldspar are replaced by NH_4^+ ammonium cationic molecular units in buddingtonite.

The specific feldspar selected for investigation is anorthite. Anorthite (abbreviated An) belongs to the plagioclase feldspar series of tectosilicate (framework silicate) minerals within the feldspar group (see Figure 1). Natural anorthites range from 90-100 mol.% An, meaning that dissolved in solid solution with $CaAl_2Si_2O_8$, may be up to 10 mol.% albite (Ab), $NaAlSi_3O_8$. In the study presented here, the interest is to synthesize a *pure alkaline-earth* feldspar, i.e., containing only Ca^{2+} cations (no alkali, Na^+ or K^+ cations incorporated in the feldspar crystal structure, as are typically found in nature). This said, the purpose of this paper is to report results of a series of

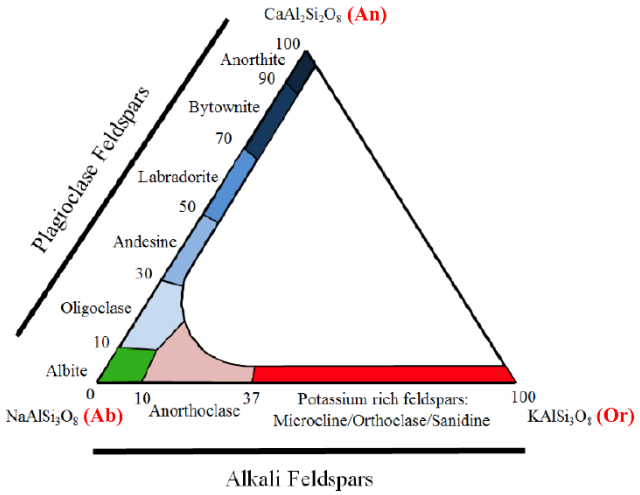

Figure 1. The feldspar anorthite – albite – orthoclase (abbreviated An – Ab – Or) ternary phase diagram. The diagram shows the plagioclase feldspar mineral series which is a solid solution series extending from end-member compound, $NaAlSi_3O_8$ (Ab), to end-member compound, $CaAl_2Si_2O_8$ (An). The diagram also shows the alkali feldspar series, a solid solution series extending from end-member compound, $NaAlSi_3O_8$ (Ab), to end-member compound, $KAlSi_3O_8$ (Or). This figure was adapted from Figure 1 in Reference [8].

synthesis and processing experiments designed to fabricate pure, highly-dense $CaAl_2Si_2O_8$ anorthite samples. The results of the synthesis experiments, which involve blending oxide powders using *dry ceramic powder processing* procedures, and the consolidation experiments to produce high-density pellets of An are reported. Here, pellet consolidation using *pressure-less sintering* versus *uniaxial hot-press sintering* procedures are compared and the results of synthesis and consolidation experiments, as determined using various materials characterization techniques, are presented.

2. Experimental Procedure

In order to properly compare powder consolidation using conventional pressure-less sintering to uniaxial hot-pressing, a detailed procedure for pre-sintering powder processing must be established. In this study, a series of powder processing steps were developed in order to facilitate the production of highly-dense, synthetic minerals via consolidation. While powder processing is not the focus this investigation, an abbreviated procedure will be presented prior to consolidation techniques.

2.1 Compound Synthesis

The constituent oxide powders used to produce the bulk powder mixture were aluminum sesquioxide (Al_2O_3, 99.95%, Alfa Aesar #42573), silicon dioxide (SiO_2, Grade 100, Fisher Chemical™ CAS: 7631-86-9), and calcium monoxide (CaO, 99.95%, Alfa Aesar #44776). Literature has addressed that these materials are hygroscopic and it is typical procedure to calcine the powders to drive off the hydrous phases prior to further processing [9, 10]. This is true for

silica and calcium oxide. Alumina did not display significant weight percent loss of water, as seen in Figure 2, and was therefore not calcined. To determine the proper calcination times and temperatures, thermal gravimetric analysis (TGA) was performed on the oxide powders at a 20°C/min rate from 25-900°C using a TA Instruments Q500 TGA; data from the TGA can be seen in Figure 2.

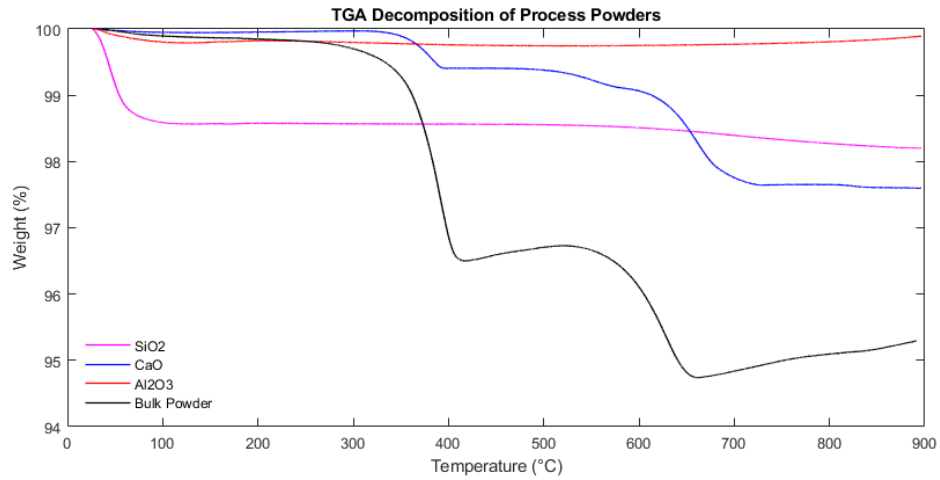

Figure 2. TGA decomposition data of raw oxide powers and bulk powder mixture.

Based on the respective TGA curves, calcination temperatures were determined to be 600°C and 800°C for SiO_2 and CaO, respectively. The powders were calcined in a muffle furnace for 30 minutes at their respective temperatures prior to weighing and mixing.

Calcined powders were weighed for the appropriate stoichiometric ratio of anorthite and then mixed and ball-milled for 30 minutes. Earlier experimentation with zirconia ball-mill containers produced sintered pellet samples with trace zirconia contaminants, therefore polypropylene vials with PMMA (polymethyl methacrylate) balls were used for high-energy milling to mechanically blend the powders. It was expected that the blended powders could hydrate during the initial powder processing, therefore a second TGA was performed under identical conditions to determine the degree of hydration. Based on the results observed in Figure 2, the bulk powder was calcined at 1000°C (70% T_m) for 3 hours directly prior to consolidation, as outlined in Figure 3.

Figure 3. Processing steps for the solid-state synthesis and consolidation of the feldspar anorthite, $CaAl_2Si_2O_8$. Processing temperatures are percentages of the melting temperature of anorthite, T_m = 1553°C [11].

2.2 Consolidation

For green body formation, calcined powder was consolidated using a Carver Press with a 13 mm diameter stainless steel evacuable pellet die. Pellets were sintered in a muffle furnace on an yttria-plated platform with a 5°C/min ramp rate, at 1300°C (90% T_m) for 12 hours and allowed to furnace cool after shut-off. Based on results of preliminary experiments, it was determined that, in the absence of a reaction barrier, green body pellets sintered on a zirconia plate reacted with the plate and resulted in new phase formation. Evidence for reaction was indicated by glossy rings surrounding each pellet on the plate. Pellets were sintered on a platinum foil or yttria powder barrier on a zirconia plate to minimize reaction between pellets and the supporting platform.

To synthesize feldspar anorthite with near theoretical density, the sintered sample (no pressure) was loaded into a 13 mm diameter graphoil-lined graphite die and consolidated in a uniaxial hot press, procured from OXY-GON. A schematic of hot-press die loading is shown in Figure 4. The temperature-pressure profile is described in the following intervals: 250°C hold for

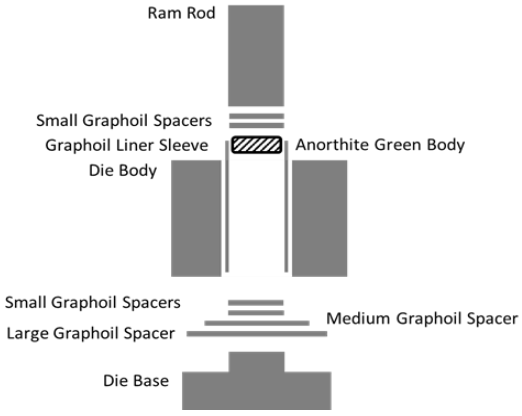

Figure 4. Schematic of graphite die loading of anorthite samples prior to hot-pressing.

10 minutes, 800°C and 0.5 ton hold for 20 minutes, 1000°C and 0.8 ton hold for 20 minutes, and 1200°C and 1 ton hold for 4 hours. The resulting pellets were polished to remove excess graphoil in preparation for further characterization.

2.3 Characterization

Volumetric density measurements were performed by measuring the diameter, thickness, and weight of green body pellets, sintered samples (no pressure), and consolidated hot-pressed pellets. These experimentally measured densities were then compared to the theoretical density of anorthite. X-ray diffraction (XRD) was conducted using a Bruker D2 Phaser and used to determine the phase of the final product. Experimental diffraction patterns were compared to a simulated powder X-ray diffraction pattern found in the Inorganic Crystal Structure Database (ICSD). Scanning electron microscopy (SEM) and energy-dispersive X-ray spectroscopy (EDXS) were performed on the pellets using a Phenom ProX SEM. Images were obtained using a backscattered electron (BSE) detector with 15 kV acceleration voltage for analysis of the microstructure and chemical composition.

3. Results

This section describes the results of SEM/EDXS, XRD, and density measurements for the samples synthesized over the course of this study. Figure 5 shows SEM micrographs of pressure-less sintered and hot-pressed anorthite samples. Both were sintered at 1300°C (90% T_m) for 12 hours. EDXS results for these samples can be found in Table 1; a cation-only analysis was performed to compare to the desired stoichiometry due to the unreliability of oxygen analysis in the EDXS

system. The oxygen content can readily be assessed because the cation constituents in anorthite (Ca, Al, Si) do not exhibit variations in their respective formal valences. Specifically, Ca is always Ca^{2+}; Al is always Al^{3+}; Si is always Si^{4+}. With this, oxygen (O) content can always be readily calculated.

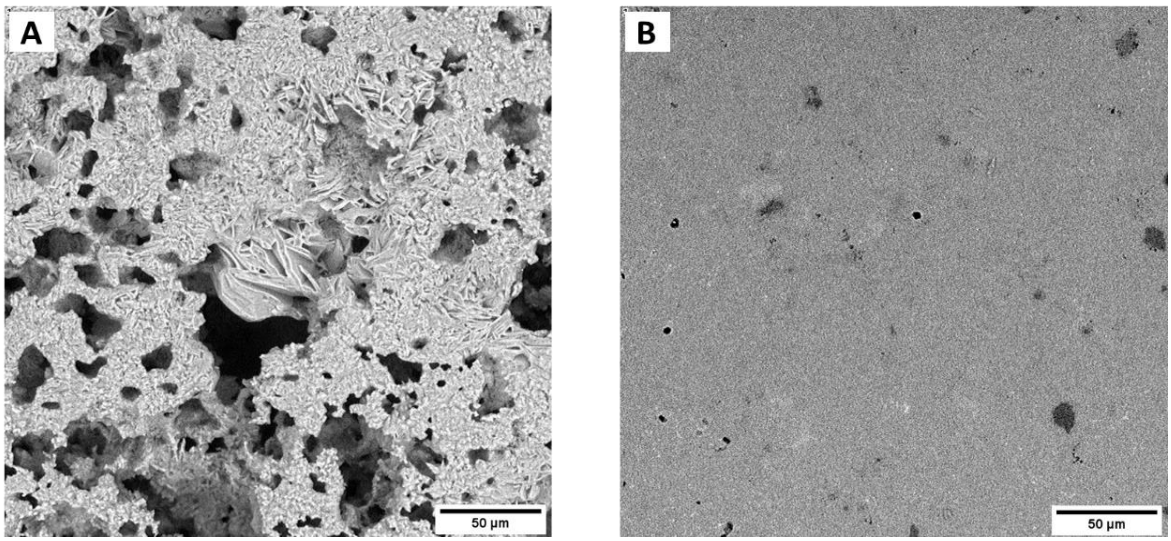

Figure 5. SEM micrographs of synthesized feldspar anorthite samples after pressure-less sintering (A) and consolidation by uniaxial hot-pressing (B). Phenom ProX, backscattered electron (BSE) Detector.

Table 1. EDXS cation analysis for pressure-less sintered and hot-pressed samples shown in Figure 3

	Theoretical (atomic %)	**Observed (atomic %)**	
		Sintered Sample (no pressure)	Hot-pressed Sample
Ca	20	20.5	17.3
Al	40	42.3	44.4
Si	40	37.2	38.3

Figure 6 shows an SEM micrograph of a biphasic region on the surface of the hot-pressed pellet sample. In the microstructure imaged in Figure 6, EDXS line scan analysis was used to conduct a cation analysis to determine phases present. Results for this analysis are displayed in Figure 7. The majority phase, characterized by lighter *Z*-contrast, is consistent with the cation composition of anorthite. The secondary phase of darker contrast is interpreted to be largely silica, potentially a silica polymorph, tridymite (Trd) or cristobalite (Crs). Note that *Z*-contrast refers to BSE image contrast that is proportional to the average atomic number of the material probed by the incident electron beam.

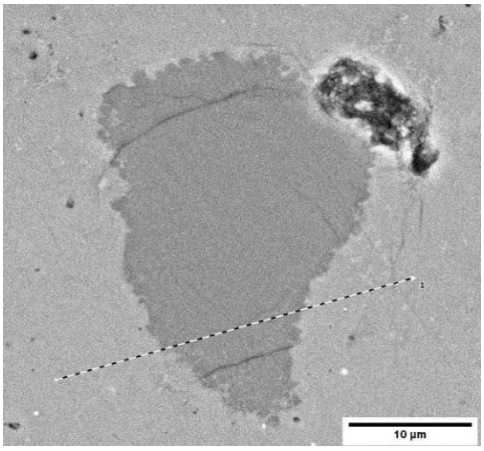

Figure 6. SEM micrograph of biphasic region on the polished hot-pressed pellet sample. Phenom ProX, backscattered electron (BSE) Detector.

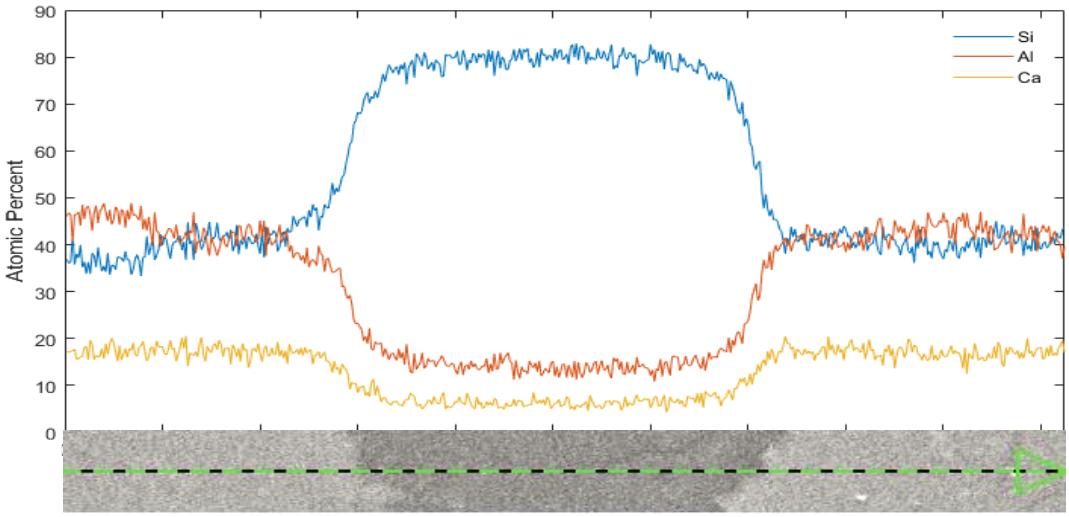

Figure 7. EDXS cation analysis of the line scan region highlighted in Figure 6.

Figure 8 shows the comparison of individual diffraction patterns of the pressure-less sintered and hot-pressed pellets, compared to simulated powder X-ray diffraction patterns for the feldspar anorthite (ICSD collection code entry #252648) [13].

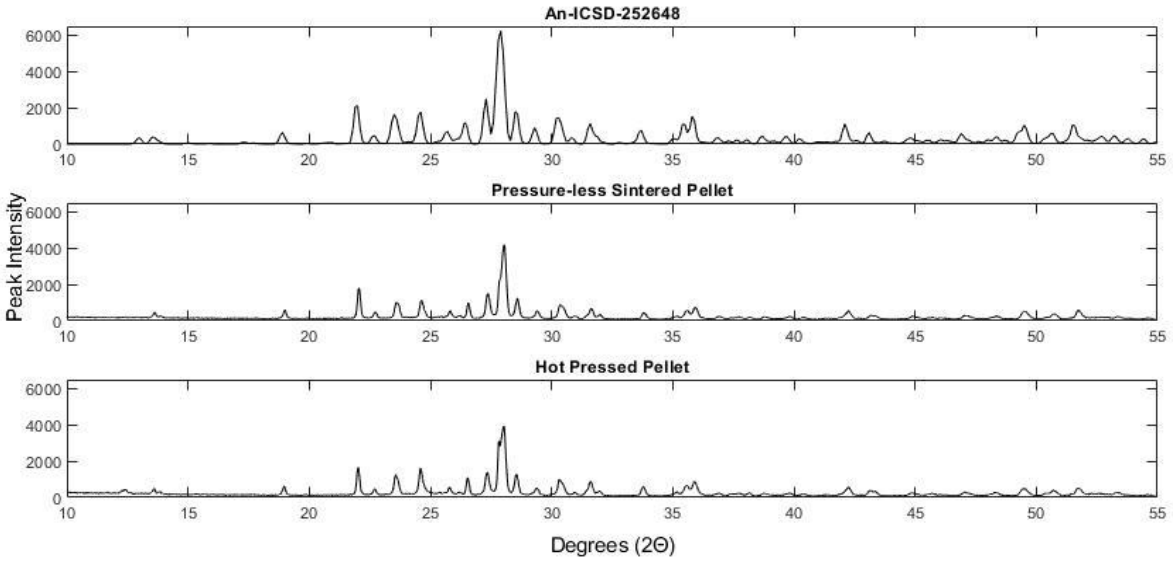

Figure 8. XRD results for pressure-less sintered and hot-pressed anorthite samples compared to a simulated powder diffraction pattern for anorthite (ICSD #252648).

Table 2 lists the average volumetric density measurements of synthesized green body pellets, pressure-less sintered samples, and consolidated hot-press pellets; the measured geometric densities were compared to the theoretical density of anorthite, 2.75 g/cm^3, and quantified as the percent of the theoretical density [12].

Table 2. Geometric density measurements for green body, pressure-less sintered, and hot-pressed pellet samples, compared to the theoretical density of anorthite, 2.75 g/cm^3.

	Green body pellet	**Sintered pellet (no pressure)**	**Hot-pressed pellet**
Geometric Density	1.37 g/cm^3	1.39 g/cm^3	2.52 g/cm^3
Percent Theoretical Density	50%	51%	92%

4. Discussion

The experiments outlined in Section 3 demonstrate that synthetic anorthite was successfully fabricated and that, using the technique of uniaxial hot-pressing, the synthesized samples were able to be consolidated to produce a high density, solid anorthite pellet. The pressure-less sintered pellet in Figure 5A displayed a highly porous, plate-like microstructure that was homogenous throughout the sample. The measured composition of this sample was 20.5% Ca, 42.3% Al, 37.2% Si (see EDXS cation analysis in Table 1). This is in good agreement with target cation composition for anorthite, i.e., 20% Ca, 40% Al, 40% Si. This suggests that a near pure anorthite mineral was synthesized.

The hot-pressed pellet sample in Figure 5B displayed a uniform microstructure with only a few surface pores. The composition of this sample was relatively constant, with second phases occurring only sporadically across the polished surface of the sample. The measured (average) composition of the hot-pressed sample was 17.3% Ca, 44.4% Al, 38.3% Si (see EDXS results, Table 1). Once again, this is close to the target for anorthite, i.e., cation ratios, Ca: Al: Si = 20%: 40%: 40%. This supports the conclusion that nearly pure anorthite was formed in this experiment. Occasional second phase regions were observed on the surface of the polished, hot-pressed sample. For instance, the SEM micrograph in Figure 6 shows a biphasic microstructural region of the hot-pressed sample. Evidence for two phases in this region is based on the observed variable contrast in the Figure 6 BSE image. This was confirmed upon measuring the chemistries of the two regions using EDXS (Figure 7). The microstructural regions of lighter BSE contrast possess compositions consistent with anorthite. The central region with darker BSE contrast exhibits much higher silicon content. The EDXS analysis (Figure 7) indicates that the cation stoichiometry of this region is approximately 80% Si, 15% Al, and 5% Ca.

XRD analyses shown in Figure 8 indicate that the feldspar anorthite was successfully synthesized in both pressure-less sintered and hot-pressed samples. This conclusion is based on the observation that the experimental XRD patterns obtained from both samples align closely with many peaks occurring in the simulated anorthite powder XRD pattern (ICSD #252648). Moreover, anorthite possesses a large crystal structure unit cell, making it possible to qualitatively examine XRD patterns for evidence of the anorthite crystalline phase. A large unit cell leads to some unusually large interatomic planar spacings, compared to simpler oxides, such as the monoxide, CaO, the sesquioxide, Al_2O_3, and the dioxide, SiO_2 (all of which have relatively small unit cells compared to anorthite). The large interplanar spacings in anorthite cause Bragg diffraction peaks to appear at very small scattering angles, 2θ, specifically in the range between 2θ = 10° - 15°. The hot-pressed sample diffraction pattern exhibits two characteristic low-angle peaks: one at 2θ = 13.03°, the other at 2θ = 13.61°. In the pressure-less sintered sample, only one low-angle peak was observed, namely, a peak at 2θ = 13.61°. Another anorthite peak at 2θ = 13.03°, corresponding to the $\{1\bar{1}0\}$ set of atomic planes with interplanar spacing, $d_{1\bar{1}0}$, should have been observed but was not. Preferential grain texture is a possible explanation for why this peak is not present in the experimental XRD pattern obtained from the pressure-less sintered sample.

The selected ICSD entry (#252648) seems to have a unit cell that is slightly larger compared to the anorthite samples produced in this study. The evidence for this is that the diffraction peaks in the simulated powder XRD pattern for ICSD-252648 are shifted to lower values of 2θ, compared to the XRD peak positions for the pressure-less sintered and hot-pressed samples [13]. The difference between the original An-ICSD-252648 simulated powder XRD pattern and the experimental patterns are likely due to Na^+ substitution for Ca^{2+} in the experimental sample upon which the #252648 entry in the ICSD database is based. The reference for this ICSD entry indicates

that this anorthite was not pure $CaAl_2Si_2O_8$, but rather was a plagioclase feldspar containing some Na+ substitution for Ca^{2+} [14]. This Na^{1+} substitution may be responsible for the approximate +2% lattice dilation (expansive dilation) of the ICSD anorthite compared to the experimental anorthite samples produced in this study.

Finally, it is useful to examine the observed differences between the sample densities achieved using the two consolidation methods examined in this study, namely pressure-less sintering versus uniaxial hot-pressing. Pressure-less sintered anorthite samples displayed low density values compared to the theoretical anorthite density of 2.75 g/cm^3 [12]. The pressure-less sintered samples achieved a density of 51% theoretical, compared to the green body density of 50% theoretical (Table 2). In other words, the pressure-less sintered samples did not achieve significant increases in density, despite formation of the anorthite mineral phase, as verified by the characterization experiments described above. Upon consolidation in a hot-press, the sample achieved approximately a 50% increase in density, reaching ~92% of the theoretical density of anorthite.

5. Conclusions

This study focused on the synthesis of the feldspar anorthite, $CaAl_2Si_2O_8$, via solid-state procedures and the densification of the as-synthesized powders using the technique of uniaxial hot-pressing. Component powders of aluminum sesquioxide (Al_2O_3), silicon dioxide (SiO_2), and calcium monoxide (CaO) were subjected to bulk powder milling, calcination, powder consolidation, and pressure-less sintering to produce high purity, homogeneous anorthite mineral samples. These samples were then hot-pressed to produce solid, high-density anorthite pellets. The densification of solid anorthite samples was monitored using geometric density

measurements. The composition and microstructure of the pressure-less sintered and hot-pressed samples were characterized by X-ray diffraction (XRD), scanning electron microscopy (SEM), and energy-dispersive X-ray spectroscopy (EDXS). It was shown that near pure anorthite was successfully synthesized and that uniaxial hot-pressing of anorthite samples yielded a solid pellet with a density 90.8% the theoretical density of $CaAl_2Si_2O_8$. Based on the results of this study, it is believed monophasic synthetic anorthite samples with a density near 100% of the theoretical density of anorthite could be produced using a wet-chemistry synthesis approach, followed by consolidation using the technique of hot-isostatic hot-pressing.

6. References

[1] Ghadiri, M., Chrzanowski, W., Rohanizadeh, R., "Biomedical applications of cationic clay minerals," Rsc Advances **5**(37) (2015) 29467-29481.

[2] Viseras, C., Cerezo, P., Sanchez, R., Salcedo, I., Aguzzi, C., "Current challenges in clay minerals for drug delivery," Applied Clay Science **48**(3) (2010) 291-295.

[3] Zhao, Y.N., "Review of the natural, modified, and synthetic zeolites for heavy metals removal from wastewater," Environmental Engineering Science **33**(7) (2016) 443-454.

[4] Zhou, Y., Zeng, H.C., "Synthesis, self-assembly, transformation, and functionalization of nanoscale artificial allophane spherules for catalytic applications," Chemistry of Materials **29**(14) (2017) 6076-6086.

[5] Goldsmith, J.R., "Gallium and germanium substitutions in synthetic feldspars," Journal of Geology **58**(5) (1950) 518-536.

[6] Flehmig, W., "Synthesis of feldspars at temperatures between 0-degrees-c - 80-degrees-c, their ordering behavior and twinning," Contributions to Mineralogy and Petrology **65**(1) (1977) 1-9.

[7] Pöter, B., Gottschalk, M., Heinrich, W., "Crystal-chemistry of synthetic k-feldspar-buddingtonite and muscovite-tobelite solid solutions," American Mineralogist **92**(1) (2007) 151-165.

[8] Harrison, A.D., Whale, T.F., Carpenter, M.A., Holden, M.A., Neve, L., O'Sullivan, D., Temprado, J.V., Murray, B.J., "Not all feldspars are equal: A survey of ice nucleating properties across the feldspar group of minerals," Atmospheric Chemistry and Physics **16**(17) (2016) 10927-10940.

[9] Bilton, M.; Brown, A.P.; Milne, S.J. "Investigating the Optimum Conditions for the Formation of Calcium Oxide, Used for CO_2 sequestration, by Thermal Decomposition of Calcium Acetate," Journal of Physics: Conference Series **371**(1) (2012) 012075.

[10] Lin, B.; Zhou, S. "Poly(Ethylene Glycol)-Grafted Silica Nanoparticles for Highly Hydrophilic Acrylic-Based Polyurethane Coatings," Progress in Organic Coatings **106** (2017) 145–154.

[11] Goldsmith, J.R. "The melting and breakdown reactions of anorthite at high pressures and temperatures." American Mineralogist, **65** (1980) 272-284.

[12] Mueller, H.J., et al. "Chapter 4: Simultaneous determination of elastic and structural properties under simulated mantle conditions using multi-anvil device MAX80." Advances in High-Pressure Technology for Geophysical Applications, (2005) 67- 94.

[13] Bergerhoff, G., Brown, I.D., "Inorganic Crystal Structure Database (ICSD)," in Crystallographic Databases," edited by F.H. Allen, G. Bergerhoff and R. Sievers. (Chester, International Union of Crystallography (IUCr), 1987), pp. 77-95.

[14] Angel, R.J., Nestola, F., "A century of mineral structures: How well do we know them?," American Mineralogist **101**(5-6) (2016) 1036-1045.